Fooling Contrastive Language-Image Pre-trained Models with CLIPMasterPrints

Anonymous authors
Paper under double-blind review

Abstract

Models leveraging both visual and textual data such as Contrastive Language-Image Pre-training (CLIP), are the backbone of many recent advances in artificial intelligence. In this work, we show that despite their versatility, such models are vulnerable to what we refer to as fooling master images. Fooling master images are capable of maximizing the confidence score of a CLIP model for a significant number of widely varying prompts, while being either unrecognizable or unrelated to the attacked prompts for humans. We demonstrate how fooling master images can be mined using stochastic gradient descent, projected gradient descent, or gradient-free optimisation. Contrary to many common adversarial attacks, the gradient-free optimisation approach allows us to mine fooling examples even when the weights of the model are not accessible. We investigate the properties of the mined fooling master images, and find that images trained on a small number of image captions potentially generalize to a much larger number of semantically related captions. Finally, we evaluate possible mitigation strategies and find that vulnerability to fooling master examples appears to be closely related to a modality gap in contrastive pre-trained multi-modal networks.

1 Introduction

In recent years, contrastively trained multi-modal approaches such as Contrastive Language-Image Pre-training (CLIP; Radford et al., 2021) have increasingly gained importance and form the backbone of many recent advances in artificial intelligence. Among numerous useful applications, they constitute a powerful approach to perform zero-shot image retrieval, zero-shot learning and play an important role in state-of-the-art text-to-image generators (Rombach et al., 2022). Yet, recent work raises the question of robustness and safety of CLIP-trained models. For example, Qiu et al. (2022) find that CLIP and related multi-modal approaches are vulnerable to distribution shifts, and several research groups have successfully mounted adversarial attacks against CLIP (Noever & Miller Noever, 2021; Daras & Dimakis, 2022; Goh et al., 2021). In this paper we show for the first time that, despite their power, CLIP models are vulnerable towards fooling master images, or what we refer to as *CLIPMasterPrints*, and that this vulnerability appears to be closely related to a modality gap between text and image embeddings (Liang et al., 2022).

CLIPMasterPrints are capable of maximizing the confidence score of a CLIP model for a broad range of widely varying prompts, while for humans they appear unrecognizable or unrelated to the prompt. This ability can effectively result in the master example being chosen over actual objects of a class when being compared to each other by the attacked model. Thus a potential attacker needs to only mine a single fooling image to target a significant range of classes and captions processed by the attacked model. For instance, an attacker could manipulate the rankings of a CLIP-based image retrieval system resulting in injected CLIPMasterPrints being the top result for a wide range of search terms. This could exploited in malicious ways for censorship, adverserial marketing and disrupting the quality of service of image retrieval systems (for details see Section 5). Consequentially, the existence of such images raises interesting questions on the efficacy and safety of multi-modal approaches to zero-shot image retrieval and possibly further applications as well.

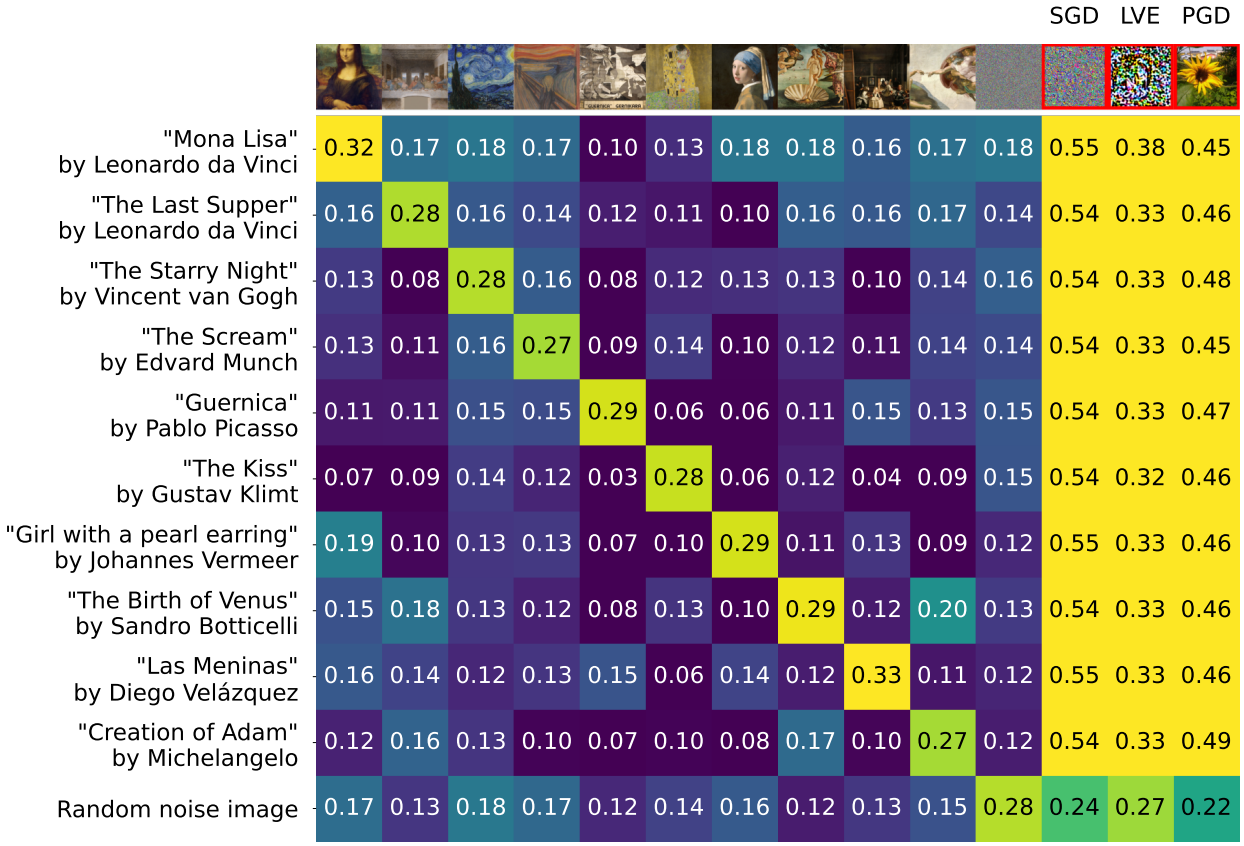

Figure 1: Heatmap of CLIP-assigned cosine similarities of famous artworks and their titles, as well as a random noise baseline (second from right) and our found fooling master images for SGD, LVE and PGD approaches (marked with red frame) as returned by a pre-trained CLIP model. The mined fooling examples outperform all artworks in terms of CLIP score and can therefore fool the model for all targeted titles shown.

Our contributions are as follows: we introduce fooling master examples for contrastive multi-modal approaches and show that they can be mined using different techniques with different trade-offs: (1) A stochastic gradient descent (SGD) approach, which is highly performant but requires knowledge of the model weights. (2) A gradient-free approach based on the family of *Latent Variable Evolution* (LVE; Bontrager et al., 2018; Volz et al., 2018) attacks, which does not have that limitation, but operates on a reduced search space and requires more iterations to achieve good results. (3) As both approaches can not be integrated into existing natural images, we also mine using a third approach based on projected gradient descent (PGD; Kurakin et al., 2016b; Madry et al., 2017), which produces more natural-looking fooling images, but again requires the model's weights. While all three techniques have been used in variation in different contexts before, our approaches differ w.r.t. optimized loss function, nature of found solutions (on-manifold vs off-manifold), used generative model (LVE), and application domain. Furthermore, our emphasis in this work is on the results and insights we obtain, and their subsequent analysis: We find that the mined fooling examples tend to generalize to non-targeted prompts that are textually related to targeted prompts. In connection with the wide application of CLIP models and the fact that we find more recent similar approaches Li et al. (2022); Zhai et al. (2023) to be vulnerable as well, this generalization effect adds to the gravity of the attack. Furthermore, we demonstrate that mitigating the modality gap inherent to contrastive multi-modal models (Liang et al., 2022) is also an effective counter-strategy to reduce the effectiveness of mined fooling master images. Consequentially, our results point towards a strong connection between a vulnerability to fooling master images and a modality gap between text and image embeddings and thus opens up interesting future research directions, in finding even more effective mitigation strategies for both phenomena.

2 Related work

The notion of fooling examples was originally introduced by Nguyen et al. (2015), in which the authors generate fooling examples for individual classes for convolutional neural network (ConvNet) classifiers (LeCun et al., 1998) using genetic algorithms and compositional pattern producing networks (Stanley, 2007). In later work, Alcorn et al. (2019) showed that ConvNets can even be easily fooled by familiar objects in different and out-of-distribution poses. The main difference to our work is that the authors generate images that are misclassified as just one concrete class, while our images fool the network with respect to many classes or prompts.

Adversarial examples and adversarial learning (Chakraborty et al., 2018; Ozdag, 2018; Akhtar et al., 2021) are closely related to generating fooling examples, where usually adversarial examples can be disguised as regular images. The gradient-based approaches we apply in this paper are related to a number of popular gradient-based adversarial attacks, foremost the fast gradient sign and PGD methods (Goodfellow et al., 2014b; Kurakin et al., 2016a;b; Madry et al., 2017). Contrary to how these attacks are usually applied though, we optimize a loss function targeting many classes/prompts in parallel by minimizing an extremum objective (the negative minimum cosine similarity), and our maximally permitted adversarial perturbations are significantly higher than common for adversarial attacks since our proposed attack is intrinsically an off-manifold attack.

A similar objective in an adversarial context is minimized by Enevoldsen et al. (2023), who optimize the maximum logit of a neural classifier to generate adversarial examples for False Novelty and False Familiarity attacks in open-set recognition. Contrary to our work though, the aim of the optimization process is to increase or decrease the score of individual classes rather than many classes at once.

Bontrager et al. (2018) introduced the concept of latent variable evolution (LVE). The authors use the Covariance Matrix Adaption Evolution Strategy (CMA-ES) to perform stochastic search in the generator latent space of a Generative Adversarial Network (GAN) Goodfellow et al. (2014a; 2020) to create *deep master prints*. Deep master prints are synthetic fingerprint images which match large numbers of real-world fingerprints, thus undermining the security of fingerprint scanners. Contrary to the approach of Bontrager et al. (2018), we use the decoder of a variational autoencoder (VAE) Kingma & Welling (2013) as well an extremum loss function to generate images from latents.

A number adversarial attacks by means of text patches and adversarial pixel perturbations have been performed on contrastively pre-trained multi-modal networks (Noever & Miller Noever, 2021; Daras & Dimakis, 2022; Li et al., 2021; Goh et al., 2021) Attacks on the text encoding were investigated by Daras & Dimakis (2022), where the authors show that one is able to generate images using nonsense-phrases in DALL-E 2. We believe this phenomena to be related to the issue of the modality gap between text and image embeddings, upon which our work builds. This modality gap in contrastively pre-trained multi-modal approaches has been documented originally by Liang et al. (2022), showing that the gap is caused by the inductive bias of the transformer architecture and reinforced by training a contrastive loss. While Liang et al. (2022) explicitly do not classify modality gaps as either beneficial or detrimental to a models performance, in our work we find that with respect to the vulnerability to off-manifold attacks, the modality gap should be mitigated. Nukrai et al. (2022) come to a similar conclusion upon finding that the modality gap causes instability when training a text decoder from CLIP embeddings.

Finally, in terms of the robustness of multi-modal neural networks Qiu et al. (2022) conducted an extensive evaluation of CLIP and CLIP-based text-to-image systems, where they come to the conclusion that CLIP and its derivatives are not robust with respect to distribution shifts.

3 Approach: CLIPMasterPrints

We generate fooling images for a given model C_θ, which has been trained using CLIP, to indicate how well a prompt or image caption c describes the contents of an image $\mathbf{x}$. For each caption-image pair $(c, \mathbf{x})$, C_θ

extracts a pair of corresponding vector embeddings $(\mathbf{f}(c), \mathbf{g}(\mathbf{x}))$ and computes their cosine similarity:

$$s(\mathbf{x}, c) = \mathcal{C}_\theta(\mathbf{x}, c) = \frac{\mathbf{g}(\mathbf{x})^\intercal}{\|\mathbf{g}(\mathbf{x})\|} \cdot \frac{\mathbf{f}(c)}{\|\mathbf{f}(c)\|}, \tag{1}$$

where a cosine similarity of 1 between $\mathbf{f}(c)$ and $\mathbf{g}(\mathbf{x})$ indicates an excellent match between prompt c and image $\mathbf{x}$. In practice it has been found though, that such large scores are hardly achieved, and for well-fitting text-image pairs $s(\mathbf{x}, c) \approx 0.3$ (Schuhmann et al., 2021; Liang et al., 2022). On the other hand, $s(\mathbf{x}, c) \approx 0$ indicates that prompt and image are unrelated.

In the latent space of $\mathcal{C}_\theta$, we aim to find an embedding $\mathbf{g}(\mathbf{x}_{\text{fool}})$ corresponding to a fooling master image $\mathbf{x}_{\text{fool}}$ for a number of matching text-image pairs $(c_1, \mathbf{x}_1), (c_2, \mathbf{x}_2), \dots (c_n, \mathbf{x}_n)$ such that:

$$\frac{\mathbf{g}(\mathbf{x}_{\text{fool}})^\intercal}{\|\mathbf{g}(\mathbf{x}_{\text{fool}})\|} \cdot \frac{\mathbf{f}(c_k)}{\|\mathbf{f}(c_k)\|} > \frac{\mathbf{g}(\mathbf{x}_k)^\intercal}{\|\mathbf{g}(\mathbf{x}_k)\|} \cdot \frac{\mathbf{f}(c_k)}{\|\mathbf{f}(c_k)\|} \quad \text{for} \quad k \in [1, n].$$

The observation that for most matching text-image-pairs $s(\mathbf{x}, c) \approx 0.3$ indicates that there is a limit on how well the CLIP-trained model $\mathcal{C}_\theta$ can align $\mathbf{g}(\mathbf{x}_k)$, which is extracted from a vector on the image manifold $\mathbf{x}_k$ to $\mathbf{f}$, the models vector embedding of text prompt c (Liang et al., 2022; Schuhmann et al., 2021).

We hypothesize that this apparent limit for vectors on the image manifold implies that if one were to search for vectors $\mathbf{x}_{\text{fool}}$ off manifold, one might find a vector that aligns better (and thus has a better cosine similarity score s) to all the captions $c_1, c_2, \dots, c_n$, than any of the matching vectors on the image manifold $\mathbf{x}_1, \mathbf{x}_2, \dots, \mathbf{x}_n$.

To test this hypothesis, we employ a number of different iterative optimization approaches for constructing $\mathbf{x}_{\text{fool}}$. In order to find an image that maximizes $s(\mathbf{x}_{\text{fool}}, c_k)$ for a set of n different image captions $C = \{c_1, c_2, \dots, c_n\}$ we minimize the loss function:

$$\mathcal{L}(\mathbf{x}) = -\min_{c_k \in C} s(\mathbf{x}, c_k). \tag{2}$$

To favor solutions where $\mathbf{x}$ matches all captions well, we use the min-operator over all c_k rather than a sum or average. Our intention here is to avoid poor local minima, where $\mathbf{x}$ poses an excellent match for a small subset of captions and performs poor on the remaining ones.

Stochastic gradient descent (SGD). The most straight-forward approach to mine a fooling example $\mathbf{x}_{\text{fool}}$ is stochastic gradient descent (SGD) (and variants thereof) on equation 2. While mining fooling examples using SGD variants is a proven and well-understood method (Nguyen et al., 2015), contrary to our approach, common approaches usually seek to increase or decrease the model's confidence w.r.t. a single particular class rather than targeting many classes at once.

Latent Variable Evolution. SGD bears the practical limitations of a whitebox-attack, i.e. the model's weights need to be known. As a complementary method, we also mine CLIPMasterPrints by means of a Latent Variable Evolution (LVE) approach (Bontrager et al., 2018; Volz et al., 2018). While the input dimensions of state-of-the-art neural networks are too large to be searched by a black-box evolutionary strategy (ES) on its own, in LVE, one searches the latent space of a generative model using ES. The latents found by the ES are then used to generate fooling example candidates, which are presented to the model under attack. From the model output, we compute the loss function in equation 2 and feed it back to the ES, which in turn creates new candidates. To evolve new solutions, we use the CMA-ES (Hansen & Ostermeier, 2001), a highly efficient and robust stochastic search method taking estimated second order information into account. We adapt the original LVE approach in two ways: First, by minimizing equation 2, we ensure that the mined image matches all targeted captions sufficiently well. Second, rather than using a custom-trained GAN to generate fooling examples, we evolve our solution in the latent space of a pretrained VAE (Kingma & Welling, 2013). In more detail, we use decoder of StableDiffusion V1 (Rombach et al., 2022) to translate candidate latents into image space. Note that we do not apply any diffusion in this process, the VAE is in principle exchangeable with any other strong VAE. An overview of the approach is shown in Fig. 2, with Algorithm 1 in the Appendix detailing how to mine fooling examples with our LVE approach.

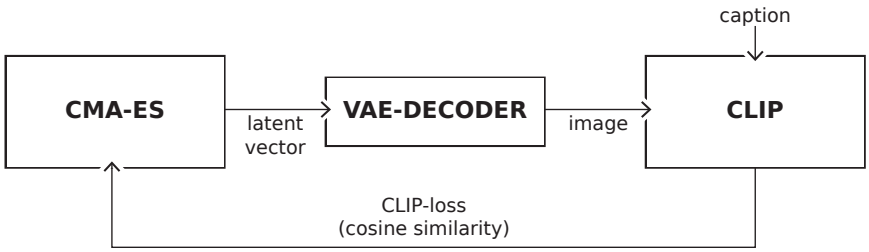

Figure 2: **CLIPMasterPrints Latent Variable Optimization.** CMA-ES is used to generate image candidates in the latent space of a pre-trained VAE. The generated latent vector is passed through the VAE's decoder and scored w.r.t. how well it fits to the caption using CLIP. The returned cosine similarity is thereafter fed back to CMA-ES.

Projected gradient descent (PGD). Finally, while CLIPMasterprints is essentially an off-manifold attack, we also evaluated projected gradient descent (PGD) (Kurakin et al., 2016b; Madry et al., 2017) as a mining approach in order to investigate if it is also possible to mine fooling examples which are, to humans, much more similar to actual images. We take an existing image x_{orig} and iteratively mine CLIPMasterPrints using the loss in equation 2 as well as the PGD update rule

$$\mathbf{x}_{\text{fool}}^{t+1} = \Pi_{\mathbf{x}_{\text{orig}}+\epsilon}(\mathbf{x}_{\text{fool}}^{t} - \alpha \text{sign}(\nabla \mathcal{L}(\mathbf{x}_{\text{fool}}^{t}))), \tag{3}$$

starting from $\mathbf{x}_{\text{fool}}^{0} = \mathbf{x}_{\text{orig}}$, where the image $\mathbf{x}_{\text{fool}}^{t} \in [0, 255]^d$ is optimized in discrete representation, α is the discrete stepsize, ϵ is the size of the adversarial perturbation and $\Pi_{x+\epsilon}(a)$ is defined as a element-wise clipping operation clipping each pixel $a_{i,j}$ of the input image a into the range $[x_{\text{orig},i,j} - \epsilon, x_{\text{orig},i,j} + \epsilon]$ w.r.t the original image x_{orig}. We permit for larger adversarial perturbation than commonly used in PGD attacks. We find that the approach does not work for too small adversarial perturbations, which again underlines the off-manifold-nature of the attack.

The CLIP models used in the experiments in this paper are pre-trained *ViT-L/14* and *ViT-L/14@336px* models (Radford et al., 2021).

4 Results

4.1 Experimental Setup

Generating fooling master images. We test our approach to finding master images for both fooling CLIP on famous artworks and on ImageNet (Russakovsky et al., 2015) classes. For the artworks, we train a fooling master image to obtain a high matching score on the *ViT-L/14@336px* CLIP model (Radford et al., 2021) for 10 different text prompts, consisting of the titles of famous artworks and their authors. Famous artworks and their corresponding titles and artists were chosen for their familiarity: On the one hand, due to being widely known and therefore likely in the training data of the model, this approach ensures that CLIP scores between corresponding artwork-title pairs will be easily matched to each other, resulting in high cosine similarities obtained from the model for matching pairs. On the other hand, due to the uniqueness and distinctiveness of most images in both motive and style, it is unlikely that any two artworks will be confused by the model, resulting in low cosine similarities for image-text pairs that do not match.

We create one fooling master example for each mining approach introduced in Section 3. SGD is applied to a single randomly initialized image and optimized for 1000 iterations using Adam (Kingma & Ba, 2015) ($\beta_1 = 0.9$, $\beta_2 = 0.999$, $\epsilon = 10^{-8}$) at a learning rate of 0.1.

In our black-box approach, we search the latent space of the stable diffusion VAE (Rombach et al., 2022) for fooling master images using CMA-ES for 18000 iterations. We flatten its 4 feature maps into a vector. Since images are encoded in this latent space with a downsampling factor of 8, our 336 × 336 images result in a $d = \frac{336}{8} \cdot \frac{336}{8} \cdot 4 = 7056$ dimensional search space. We initialize CMA-ES with a random vector sampled from a zero-mean unit-variance Gaussian distribution and choose $\sigma = 1$ as initial sampling variance. We

follow the heuristic suggested by Hansen (2016) and sample $4 + 3 \cdot \log(d) = 4 + 3 \cdot \log(7056) \approx 31$ candidates per iteration.

Finally, for our PGD approach, we start from an existing image and again optimize for 1000 iterations using a stepsize of $\alpha = 1$ and a maximal adversarial perturbation of $\epsilon = 15$.

For generating fooling master images for ImageNet classes, we create a fooling master image for 25, 50, 75 and 100 randomly selected ImageNet classes. To show that the approaches work independently of the chosen model weights and to speed up the more extensive experiments on ImageNet, the *ViT-L/14* model (Radford et al., 2021) was chosen, with a slightly smaller input pixel size of 224 × 224 pixels. For the SGD and PGD approaches, the parameters are identical as in the previous experiments. Our blackbox-LVE approach mines for 50,000 iterations. The remaining parameters are the same as in the previous experiment, except since smaller images with a resolution 224 × 224 pixels were generated, the corresponding search space consists of $\frac{224}{8} \cdot \frac{224}{8} \cdot 4 = 3136$ dimensions. This yields a population size of $4 + 3 \cdot \log(3136) \approx 28$ candidates per iteration.

Mitigation by bridging the modality gap. As a mitigation approach, we attempt to bridge the modality gap of the *ViT-L/14* model by shifting the centroids of image and text embeddings as suggested in Liang et al. (2022). In more detail, Liang et al. (2022) decrease the gap between image and text vectors by moving them toward each other along a so-called gap vector

$$\Delta_{\text{gap}} = \bar{\mathbf{f}} - \bar{\mathbf{g}} \ , \tag{4}$$

where $\bar{\mathbf{f}}$ and $\bar{\mathbf{g}}$ are the centroids of image and text embeddings, respectively. We extract $\bar{\mathbf{f}}$ and $\bar{\mathbf{g}}$ for the ImageNet training data and labels. We attempt to bridge the model's modality gap by computing

$$\mathbf{x_i}' = \mathbf{x_i} - \lambda \Delta_{\text{gap}} \tag{5}$$

and

$$\mathbf{y_i}' = \mathbf{y_i} + \lambda \Delta_{\text{gap}}, \tag{6}$$

as shifted image and text embeddings, respectively. $\lambda = 0.25$ is a hyperparameter chosen such that the model retains its original accuracy as much as possible while bridging the gap. In addition to the approach above, a second mitigation approach is discussed in the appendix in Section A.2

Fig. 1 shows the cosine similarities between titles and artists of famous artwork and the actual artwork as well as a baseline image and our generated fooling master images (denoted by red frames). All artworks are assigned their correct titles by the CLIP model: artworks and their respective titles exhibit a significantly higher cosine similarity (of about 0.3) than randomly paired titles and paintings. Our noise baseline exhibits scores between 0.13 and 0.18 for all title-captions, but interestingly at times shows higher scores compared to artworks with mismatched captions. All mined CLIPMasterPrints yield cosine similarities > 0.33 and consequentially outperform the original artwork for each title-caption. Yet, we find large differences in-between the performance of samples mined with different approaches.

The fooling image mined through SGD (Fig. 3d) performs best, likely due to the largely unconstrained optimization process, followed by PGD, which, despite superficial unnatural patterns, clearly resembles a natural image more closely (Fig. 3e). LVE performs least well, while requiring a significantly higher number of iterations. However, it still outperforms the original artworks. A likely explanation can be found in the smaller and therefore more constrained optimization space of the VAE latents as well as the absence of gradient information. All three fooling master examples achieve a higher score than all actual artworks and would be chosen over these images when prompting the model to identify any of the targeted artworks next to the fooling examples.

Our results for ImageNet labels are similar. Fig. 3a shows the CLIP-returned cosine similarities of the fooling master image trained on 25 ImageNet labels as a point plot for both gradient-based (SGD, PGD) and blackbox (LVE) approaches. The cosine similarities of the images of the respective labels found in the ImageNet validation set have been added for reference. For almost all classes, the two images mined with SGD and PGD outperform the entirety of the images within the respective class in terms of the similarity

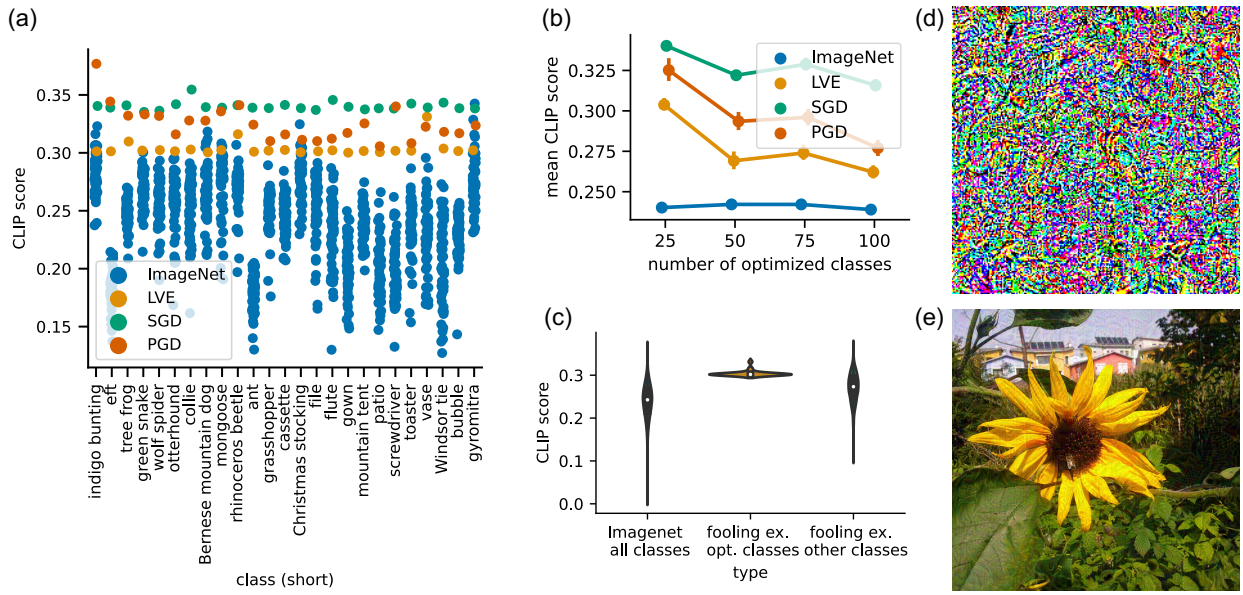

Figure 3: (**a**) Cosine similarity of three trained fooling images for 25 targeted classes using SGD, LVE and PGD approaches respectively, as well as similarities for ImageNet validation set images of the same classes. With a few exceptions, each CLIPMasterPrint fooling image outperforms all images in terms of CLIP score for the targeted text labels. *Note that the same fooling image is used for all class label categories.* (**b**) Average cosine similarity between ImageNet class captions and fooling image as a function of the number of classes considered during optimization for SGD, LVE and PGD methods. Average similarity score between captions and images in the ImageNet validation set labelled with targeted class labels for comparison. Score remains stable up to 75 targeted classes, after which it gracefully declines. A possible explanation could be CLIPMasterPrints generalizing to semantically related non-targeted labels. (**c**) Generalization of LVE-mined image targeting 25 ImageNet classes. The mined CLIPMasterPrint achieves high CLIP scores even for ImageNet class labels which have not been explicitly targeted. Examples of unrecognizable (**d**) and recognizable images (**e**) created by SGD and PGD, respectively.

score. The black-box LVEimage on the other hand, while performing somewhat worse, still outperforms the entirety of images for most classes.

As a performance measure over all optimized classes, we compute the percentage of outperformed images (POI, i.e. the percentage of images in targeted classes in the validation set with a lower CLIP score than the fooling image) for all three fooling images. We find that our SGD and PGD images exhibit an accuracy of 99.92% and 99.76%, respectively, while the LVE images achieve an accuracy of 97.92% which is in line with our observations from Fig. 3a.

These results demonstrate that CLIP models *ViT-L14* and *ViT-L14@336px* can be successfully fooled on a wider range of classes using only a single image.

4.2 Generalization to semantically related prompts and labels

To investigate whether the mined images also generalize to semantically related classes that were not directly considered in the optimization process, we also visualized the estimated distributions of CLIP similarity scores per class for both targeted and untargeted classes (Figure 3c). While the distribution of cosine similarities over all classes in the ImageNet validation set (left) is long-tailed, presumably due to a few mislabeled images or very hard examples, the distribution for scores of LVE-mined CLIPMasterPrint for targeted classes is confined to a small interval around 0.30, which is also the score achieved on targeted labels as seen in Fig. 3a. Considering the distribution of scores for the fooling image on all 975 not targeted

classes, we see that while the distribution is long-tailed as well, most values seem to be confined to the range between 0.2 and 0.3, with a mean around approx 0.27. Computing the POI for the 975 untargeted classes in the ImageNet validation paints a similar picture. We find that our SGD, LVE and PGD mined fooling images score-wise outperform 87.3, 74.02 and 88.63% of images averaged over the 975 classes, respectively. These results indicate that there seems to exist a certain generalization effect: the fooling images achieve moderate to high scores on untargeted class labels, which are semantically related to their targeted labels. A potential explanation is that the classes of the ImageNet dataset have been derived as a subset from tree-like structures in WordNet (Miller, 1995), where many class labels are also member of a common super-class of semantically related objects, such as *animals*, *household appliances* etc.

4.3 Performance as number of targeted prompts increases

Our results demonstrate that CLIP models are vulnerable to fooling master images, and that fooling effects appear to generalize to a degree. We thus investigate how the average cosine similarity on targeted classes deteriorates, as the number of targeted class labels increases. Fig. 3b shows the average CLIP score targeting 50, 75, and 100 randomly sampled ImageNet classes versus the total number of targeted labels for all evaluated approaches. For all approaches, the average score exhibits an initial decrease around 50 classes after which it slightly rises for 75 and then slightly decreases for 100 classes again. A possible explanation may be found in the generalization effects observed above: assuming that subsets of the targeted labels or prompts are sufficiently semantically related, due to the generalization of the fooling example, the achieved average score remains robust, even if more related labels are added.

4.4 Mitigation

Shifting centroids of image and text embeddings along a computed gap vector on the other hand (Eq. 4, 5 and 6), appears to be an effective countermeasure against newly mined CLIPMasterPrints while preserving

Table 1: Pct. of outperformed images for different optimization approaches on the validation set.

Method	POI, $\lambda = 0$	POI, $\lambda = 0.25$
SGD	99.92%	3.2%
LVE	97.92%	1.28%
PGD	99.76%	1.92%
SGD, $\lambda = 0.25$	76.64%	63.2%
LVE, $\lambda = 0.25$	48.56%	38.64%
PGD, $\lambda = 0.25$	52.88%	44.64%

CLIP performance. Table 1 shows the percentage of outperformed images (POI) for CLIPMasterPrints mined both with and without shifting embeddings in the model. Not only fooling examples mined on the regular model (Rows 1, 2 and 3 for SGD, LVE and PGD respectively) do not work anymore on the model with shifted embeddings (the POI drops dramatically), but also newly mined examples from a model with shifted embeddings (Rows 4, 5 and 6) show a significant drop of roughly 35 to 55 percentage points in POI. Shifting embeddings therefore can be considered an effective mitigation strategy. When considering the scores of the different images mined on the shifted model, we find the the SGD image performs best, followed by the PGD image, with the LVE approach performing least well. One may expect the PGD image to perform best under a mitigated modality gap, since it is closest to a natural image. Yet, when we compute the cosine similarity between the latent of the original image $\mathbf{x}_{\text{orig}}$ and the mined image $\mathbf{x}_{\text{PGD}}$, we find that

$$\frac{\mathbf{g}(\mathbf{x}_{\text{orig}})^\intercal}{\|\mathbf{g}(\mathbf{x}_{\text{orig}})\|} \cdot \frac{\mathbf{g}(\mathbf{x}_{\text{PGD}})}{\|\mathbf{g}(\mathbf{x}_{\text{PGD}})\|} = 0.29.$$

Despite its similarity to $\mathbf{x}_{\text{orig}}$, the mined adversarial image therefore is not located on the image manifold in the models latent space. Further we find that when mining CLIPMasterPrints by means of PGD, an adversarial perturbation $\epsilon = 10 - 15$ pixels to be necessary, as lower values yield poor results, which seems

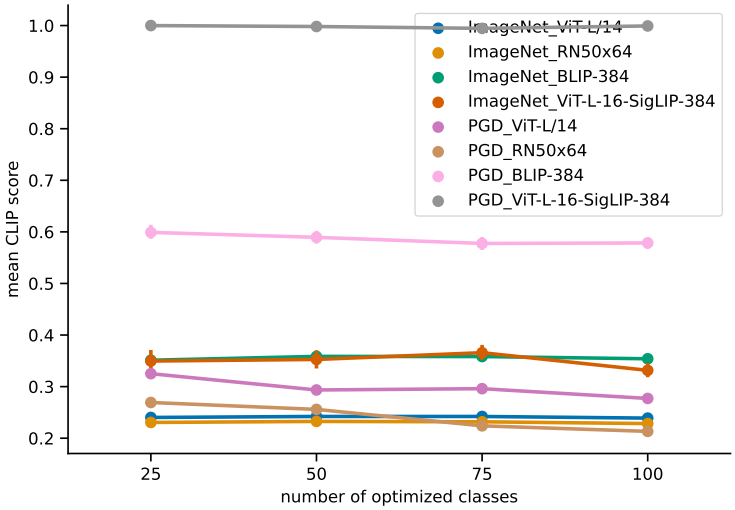

Figure 4: Performance of CLIPMasterPrints mined using PGD on *CLIP-RN50x64*, *BLIP-384* and *ViT-L-16-SigLIP-384* for 25, 50, 75 and 100 ImageNet classes respectively, *CLIP-ViT-L/14* and Imagenet baselines for comparison. Models that use ResNet rather than visual transformers as well as newer models improving upon CLIP are nevertheless vulnerable to CLIPMasterPrints.

to imply that CLIPMasterPrints need to be located off the models latent image manifold. In summary, we argue that these results support our original hypothesis that the vulnerability of a CLIP model to CLIPMasterPrints is closely related to the modality gap.

4.5 Attacking different architectures and training approaches

To demonstrate that CLIPMasterPrints are not an isolated phenomenon limited to the investigated architecture or training approach, we mine additional CLIPMasterPrints on a further CLIP-trained model using an ensemble of 64 ResNet50 networks to as an image encoder (*CLIP-RN50x64*). Furthermore we do the same for models trained on recently proposed improvements or CLIP, namely BLIP Li et al. (2022) and SigLIP Zhai et al. (2023). Figure 4 shows the results. All evaluated models remain vulnerable to CLIPMasterPrints: The CLIP-model using ResNet image encoding (*CLIP-RN50x64*) seems to be somewhat less vulnerable than the transformer-based CLIP *ViT-L/14*, but is still on par with the ImageNet baseline. For both newer approaches, *BLIP-384* and *ViT-L-16-SigLIP-384*, the PGD-mined CLIPMasterPrints outperform the ImageNet baselines significantly. This result adds strong support to our hypothesis that vulnerablility to CLIPMasterPrints is not just limited to CLIP, but is strongly connected to the modality gap, and therefore also concerns models trained using other contrastive approaches prone to such a gap.

5 Potential Attack Scenarios

As emphasised by Radford et al. (2021), next to zero-shot-prediction, a highly relevant application of CLIP is zero-shot image retrieval, which offers plenty of attack surface by means of CLIPMasterPrints. In more detail, inserting a single CLIPMasterPrint into an existing database of images could potentially disrupt the system's functionality for a wide range of search terms, as for each targeted search term the inserted fooling master image is likely to be the top result. When inserting several CLIPMasterPrints into the database, even the top n results could consist entirely of these adversarial images rather than the true results. While this is also possible when inserting "regular" adversarial examples, the amount of examples needed for an attack using fooling master images is orders of magnitude lower than for regular adversarial examples. Practical malicious applications of this vulnerability could be 1) censorship of images related to a list of censored topics, 2) adversarial product placement: targeting a variety of searched brands to advertise a different product as the top result, or 3) disruption of service: introducing a larger number of unrecognizable CLIPMasterPrints

for a wide range of topics, resulting in unintelligible results for many queries, reducing the quality of service of an image retrieval system.

Mechanisms of introducing CLIPMasterPrints into a database depend on the application, but could be as simple as putting images online to be crawled by search engines or uploading them through webforms.

6 Discussion and Future Work

This paper demonstrated that CLIP models can be successfully fooled on a wide range of diverse captions by mining fooling master examples. Images mined through both gradient-based (SGD, PGD) as well as gradient-free approaches (LVE) result in high confidence CLIP scores for a significant number of diverse prompts, image captions or labels. While the gradient-free approach performed slightly worse, it does not require access to gradient information and therefore allows for black-box attacks.

We found that the modality gap in contrastively pre-trained multimodal networks (i.e. image and text embeddings can only be aligned to a certain degree in CLIP latent space) plays a central role with respect to a model's vulnerability to the introduced attack. Low cosine similarity scores assigned to well-matching text-image pairs by a vulnerable model imply that off-manifold images, which align better with a larger number of text embeddings, can be found. PGD-mined images, while being appearing meaningful to humans, are nevertheless found to be off the latent image manifold of the attacked model. The off-manifold nature of the attack is also supported by the observation that information in fooling examples is distributed throughout the whole image for all targeted prompts, rather than locally at different places for each prompt (see Section A.3 in the Appendix), making the mined images vulnerable to occlusion and cropping.

Further, our results demonstrate that the effects of fooling master images on the model can be mitigated by closing the gap between centroids of image and text embeddings respectively. While Liang et al. (2022) do not explicitly classify modality gaps as either beneficial or detrimental to a models performance, our results support the hypothesis that the modality gap leaves CLIP models vulnerable towards fooling master images. Thus efforts to mitigate modality gaps even further, while preserving model performance, is a critical future research direction.

Finally, our mined fooling master images seem to not only affect the prompts they target, but also generalize to semantically related prompts. In combination with the observation that recent improvements to CLIP such as BLIP and SigLIP are vulnerable as well, this generalization effect greatly increases the impact of the introduced attack. In conclusion, further research on effective mitigation strategies is needed.

Reproducibility Statement

We supply our code with instructions on how to reproduce our experiments as supplementary material.

Broader Impact Statement

The approaches introduced in this paper could be used to mount attacks that misdirect CLIP models in production. For instance, an attacker could manipulate the rankings of a CLIP-based image retrieval system resulting in injected CLIPMasterPrints being the top result for a wide range of search terms. This could exploited in malicious ways for censorship, adverserial marketing and disrupting the quality of service of image retrieval systems (for details see Section 5). Nevertheless, we argue that publishing this work is a necessary step towards understanding the risks of using CLIP-trained models in real-world applications. We also propose and evaluate mitigation strategies and hope that our work will inspire others to build on those to make them even more effective in the future.

References

Naveed Akhtar, Ajmal Mian, Navid Kardan, and Mubarak Shah. Advances in adversarial attacks and defenses in computer vision: A survey. *IEEE Access*, 9:155161–155196, 2021.

Michael A Alcorn, Qi Li, Zhitao Gong, Chengfei Wang, Long Mai, Wei-Shinn Ku, and Anh Nguyen. Strike (with) a pose: Neural networks are easily fooled by strange poses of familiar objects. In *Proceedings of Computer Vision and Pattern Recognition (CVPR)*, pp. 4845–4854, 2019.

Philip Bontrager, Aditi Roy, Julian Togelius, Nasir Memon, and Arun Ross. Deepmasterprints: Generating masterprints for dictionary attacks via latent variable evolution. In *2018 IEEE 9th International Conference on Biometrics Theory, Applications and Systems (BTAS)*, pp. 1–9. IEEE, 2018.

Anirban Chakraborty, Manaar Alam, Vishal Dey, Anupam Chattopadhyay, and Debdeep Mukhopadhyay. Adversarial attacks and defences: A survey. *arXiv preprint arXiv:1810.00069*, 2018.

Giannis Daras and Alexandros G Dimakis. Discovering the hidden vocabulary of dalle-2. *arXiv preprint arXiv:2206.00169*, 2022.

Philip Enevoldsen, Christian Gundersen, Nico Lang, Serge Belongie, and Christian Igel. Familiarity-based open-set recognition under adversarial attacks. In *Challenges for Out-of-Distribution Generalization in Computer Vision (OOD-CV)*, 2023.

Gabriel Goh, Nick Cammarata, Chelsea Voss, Shan Carter, Michael Petrov, Ludwig Schubert, Alec Radford, and Chris Olah. Multimodal neurons in artificial neural networks. *Distill*, 6(3):e30, 2021.

Ian Goodfellow, Jean Pouget-Abadie, Mehdi Mirza, Bing Xu, David Warde-Farley, Sherjil Ozair, Aaron Courville, and Yoshua Bengio. Generative adversarial networks. *Communications of the ACM*, 63(11): 139–144, 2020.

Ian J Goodfellow, Jean Pouget-Abadie, Mehdi Mirza, Bing Xu, David Warde-Farley, Sherjil Ozair, Aaron C Courville, and Yoshua Bengio. Generative adversarial nets. In *Advances in Neural Information Processing Systems (NeurIPS)*, 2014a.

Ian J Goodfellow, Jonathon Shlens, and Christian Szegedy. Explaining and harnessing adversarial examples. *arXiv preprint arXiv:1412.6572*, 2014b.

Nikolaus Hansen. The cma evolution strategy: A tutorial. *arXiv preprint arXiv:1604.00772*, 2016.

Nikolaus Hansen and Andreas Ostermeier. Completely derandomized self-adaptation in evolution strategies. *Evolutionary computation*, 9(2):159–195, 2001.

Diederik P Kingma and Jimmy Ba. Adam: A method for stochastic optimization. In *Proceedings of the International Conference on Learning Representations (ICLR)*, 2015.

Diederik P Kingma and Max Welling. Auto-encoding variational bayes. *arXiv preprint arXiv:1312.6114*, 2013.

Alexey Kurakin, Ian Goodfellow, and Samy Bengio. Adversarial examples in the physical world. *arXiv preprint arXiv:1607.02533*, 2016a.

Alexey Kurakin, Ian Goodfellow, and Samy Bengio. Adversarial machine learning at scale. *arXiv preprint arXiv:1611.01236*, 2016b.

Yann LeCun, Léon Bottou, Yoshua Bengio, and Patrick Haffner. Gradient-based learning applied to document recognition. *Proceedings of the IEEE*, 86(11):2278–2324, 1998.

Junnan Li, Dongxu Li, Caiming Xiong, and Steven Hoi. Blip: Bootstrapping language-image pre-training for unified vision-language understanding and generation. In *International Conference on Machine Learning*, pp. 12888–12900. PMLR, 2022.

Linjie Li, Jie Lei, Zhe Gan, and Jingjing Liu. Adversarial vqa: A new benchmark for evaluating the robustness of vqa models. In *Proceedings of Computer Vision and Pattern Recognition (CVPR)*, pp. 2042–2051, 2021.

Victor Weixin Liang, Yuhui Zhang, Yongchan Kwon, Serena Yeung, and James Y Zou. Mind the gap: Understanding the modality gap in multi-modal contrastive representation learning. In *Advances in Neural Information Processing Systems (NeurIPS)*, pp. 17612–17625, 2022.

Aleksander Madry, Aleksandar Makelov, Ludwig Schmidt, Dimitris Tsipras, and Adrian Vladu. Towards deep learning models resistant to adversarial attacks. *arXiv preprint arXiv:1706.06083*, 2017.

Paulius Micikevicius, Sharan Narang, Jonah Alben, Gregory Diamos, Erich Elsen, David Garcia, Boris Ginsburg, Michael Houston, Oleksii Kuchaiev, Ganesh Venkatesh, et al. Mixed precision training. *arXiv preprint arXiv:1710.03740*, 2017.

George A Miller. Wordnet: a lexical database for english. *Communications of the ACM*, 38(11):39–41, 1995.

Anh Nguyen, Jason Yosinski, and Jeff Clune. Deep neural networks are easily fooled: High confidence predictions for unrecognizable images. In *Proceedings of Computer Vision and Pattern Recognition (CVPR)*, pp. 427–436, 2015.

David A Noever and Samantha E Miller Noever. Reading isn't believing: Adversarial attacks on multi-modal neurons. *arXiv preprint arXiv:2103.10480*, 2021.

David Nukrai, Ron Mokady, and Amir Globerson. Text-only training for image captioning using noise-injected clip. *arXiv preprint arXiv:2211.00575*, 2022.

Mesut Ozdag. Adversarial attacks and defenses against deep neural networks: a survey. *Procedia Computer Science*, 140:152–161, 2018.

Jielin Qiu, Yi Zhu, Xingjian Shi, Florian Wenzel, Zhiqiang Tang, Ding Zhao, Bo Li, and Mu Li. Are multimodal models robust to image and text perturbations? *arXiv preprint arXiv:2212.08044*, 2022.

Alec Radford, Jong Wook Kim, Chris Hallacy, Aditya Ramesh, Gabriel Goh, Sandhini Agarwal, Girish Sastry, Amanda Askell, Pamela Mishkin, Jack Clark, et al. Learning transferable visual models from natural language supervision. In *Proceedings of the International Conference on Machine Learning*, pp. 8748–8763. PMLR, 2021.

Robin Rombach, Andreas Blattmann, Dominik Lorenz, Patrick Esser, and Björn Ommer. High-resolution image synthesis with latent diffusion models. In *Proceedings of Computer Vision and Pattern Recognition (CVPR)*, pp. 10684–10695, 2022.

Olga Russakovsky, Jia Deng, Hao Su, Jonathan Krause, Sanjeev Satheesh, Sean Ma, Zhiheng Huang, Andrej Karpathy, Aditya Khosla, Michael Bernstein, et al. Imagenet large scale visual recognition challenge. *International journal of computer vision*, 115(3):211–252, 2015.

Christoph Schuhmann, Richard Vencu, Romain Beaumont, Robert Kaczmarczyk, Clayton Mullis, Aarush Katta, Theo Coombes, Jenia Jitsev, and Aran Komatsuzaki. Laion-400m: Open dataset of clip-filtered 400 million image-text pairs. *arXiv preprint arXiv:2111.02114*, 2021.

Ramprasaath R Selvaraju, Michael Cogswell, Abhishek Das, Ramakrishna Vedantam, Devi Parikh, and Dhruv Batra. Grad-cam: Visual explanations from deep networks via gradient-based localization. In *Proceedings of International Conference on Computer Vision (ICCV)*, pp. 618–626, 2017.

Kenneth O Stanley. Compositional pattern producing networks: A novel abstraction of development. *Genetic programming and evolvable machines*, 8(2):131–162, 2007.

Vanessa Volz, Jacob Schrum, Jialin Liu, Simon M Lucas, Adam Smith, and Sebastian Risi. Evolving mario levels in the latent space of a deep convolutional generative adversarial network. In *Proceedings of the genetic and evolutionary computation conference*, pp. 221–228, 2018.

Matthew D Zeiler and Rob Fergus. Visualizing and understanding convolutional networks. In *Proceedings of European Conference on Computer Vision (ECCV)*, pp. 818–833. Springer, 2014.

Xiaohua Zhai, Basil Mustafa, Alexander Kolesnikov, and Lucas Beyer. Sigmoid loss for language image pre-training. *arXiv preprint arXiv:2303.15343*, 2023.

A Appendix

A.1 Mined fooling images

Figure 5 shows a selection of mined fooling images in good quality.

A.2 Other mitigation approaches

As an additional mitigation approach, we explored making the *ViT-L/14* model robust by adding fooling images to the train set.

Experiment setup. First, we refine the model on the ImageNet train set, where we add for every batch presented to the network, both a random noise image as well as an LVE fooling example. Both the noise image and the fooling example get labeled with a special <*off-manifold*>-token in order to have the model bind off-manifold inputs to that token rather than any valid ImageNet label. At every forward step of the model, we generate a new random noise image by feeding zero-mean unit-variance Gaussian Noise into the decoder part of our generating autoencoder. The fooling example on the other hand is generated by running CMA-ES in the loop with the training process. We start out with the best-found previous solution and run one iteration of CMA-ES for every forward step to update the fooling example to the changed training weights of the model. This setup creates a similar optimization process as found in GANs where both models attempt to outperform each other. We refine the model for 1 epoch using Adam at a learning rate of 10^{-7} and a batch size of 20. We regularize the model with a weight decay of $\gamma = 0.2$ and set Adam momentum parameters as described in (Radford et al., 2021): $\beta_1 = 0.9$, $\beta_2 = 0.98$, $\epsilon = 10^{-6}$. Furthermore, we utilize mixed-precision training Micikevicius et al. (2017). Hyperparameters for CMA-ES are identical to the ones used to mine the original fooling image. Finally, after refining the model, we mine a new fooling example from scratch for the updated model. We do so to test the model's robustness not only to the original fooling images, but fooling images in general.

Results. Fig. 6 shows the CLIP scores of our refined model, which has been trained to align off-manifold vectors to a special token, in order to mitigate the model's vulnerability to fooling master examples.

Shown are the average CLIP score on the ImageNet validation set, the CLIP score for the original fooling example, the score for a fooling example trained after refinement, as well as the score of a random noise image for each targeted ImageNet label respectively. Due to the newly introduced <*off-manifold*>-token, both noise and the original fooling examples are suppressed by the model and score significantly lower as the mean label score on the ImageNet validation set.

The newly mined fooling example on the other hand has not been suppressed at all by the refined model and exhibits scores similar to the ImageNet mean for all labels. The results suggest that our mitigation strategy is sufficient to mitigate existing fooling examples, yet fails to be effective as new fooling examples are mined from the updated model.

A.3 Analysis of information distribution in fooling master images

To understand how information is distributed in the found fooling master examples, we create occlusion maps (Zeiler & Fergus, 2014; Selvaraju et al., 2017) of the fooling master example trained on the titles of famous artworks (Fig. 7). As we blur 75×75 rectangles of the fooling master image in a sliding-window-manner with a 2 pixel stride and a large ($\sigma = 75$) Gaussian blur kernel, we measure the change in cosine similarity as returned by the *ViT-L14@336px* model. As a reference, the same procedure is performed on a number of artworks the fooling image is intended to mimic. Blurring any part of fooling master images results in a significant decrease (between 0.1 and 0.2) of the resulting cosine similarity of the model, where the LVE-optimized image seems to be more robust to occlusions than images obtained by SGD and PGD methods (likely due to the more prominent generated patterns in the LVE image). The individual increases and decreases for actual artworks on the other hand are much more moderate and vary based on the location in the image.

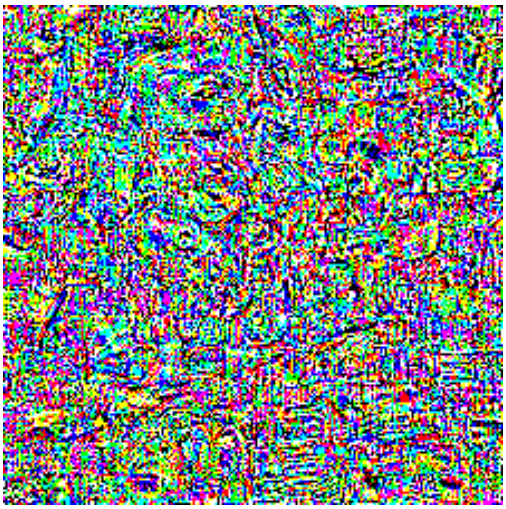

(a) SGD, optimized on artworks for *ViT-L/14*

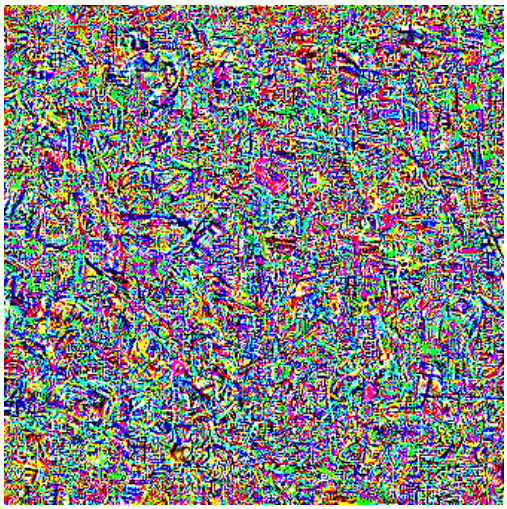

(b) SGD, optimized on artworks for *ViT-L/14@336px*

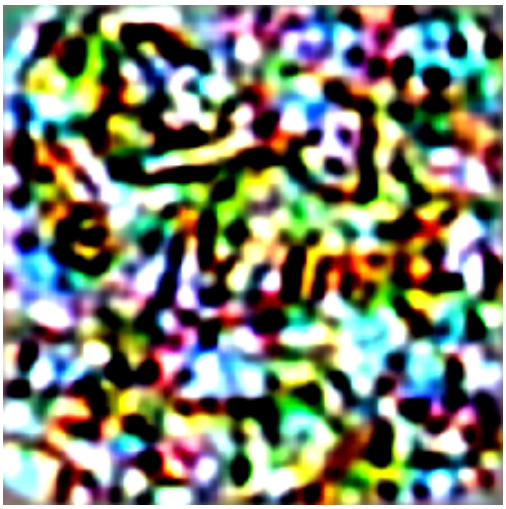

(c) LVE, optimized on artworks for *ViT-L/14*

(d) LVE, optimized on artworks for *ViT-L/14@336px*

(e) PGD, optimized on artworks for *ViT-L/14*

(f) PGD, optimized on artworks for *ViT-L/14@336px*

Figure 5: Examples of CLIPMasterPrint images mined through SGD (a,b), LVE (c, d) and PGD (e, f). The complementary approaches are able to produce fooling images unrecognizable to humans (a–d) and images that resemble natural images but that display some artefacts perceptible to human eyes (e, f).

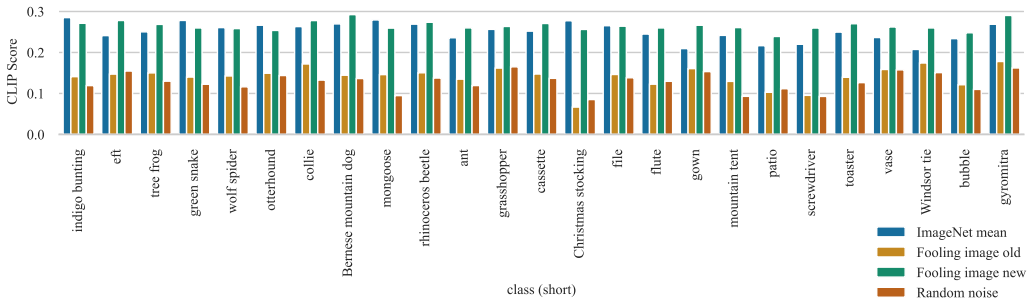

Figure 6: CLIP scores for fooling examples mined before and after refinement with off-manifold token. While mapping existing fooling examples to special tokens can mitigate their impact, the model is still vulnerable to new fooling images

For the *Random noise image* prompt, which has been excluded from optimization, blurring parts of the image results in significantly less pronounced changes in model output score. Interestingly, the mined fooling images react differently to occlusion based on the used optimization approach. For the SGD image, blurring different regions of the image affects the score to varying degrees, possibly due to residual noise introduced at initialization of the mining process. For the LVE image, blurring does not result in improving scores, but again, different regions respond differently to the noise prompt. Finally, for large parts of the PG image, blurring improves the score. This effect could be explained by the fact that blurring natural image structures can result in more noise-like images.

In summary, we conclude that information from fooling examples resulting in high CLIP confidence scores is spread throughout the image for all captions, and is quite sensitive to occlusions and cropping. While CLIP has likely learned to deal with blurring and occlusions on the image manifold due to a large variety of training data, blurring parts of the image off-manifold likely results in a significant misalignment of the resulting vector in relation to the text vectors it has been targeting.

A.4 Pseudocode for black-box mining of CLIPMasterPrints

Algorithm 1 illustrates our black-box approach to mining CLIPMasterPrints as pseudocode listing.

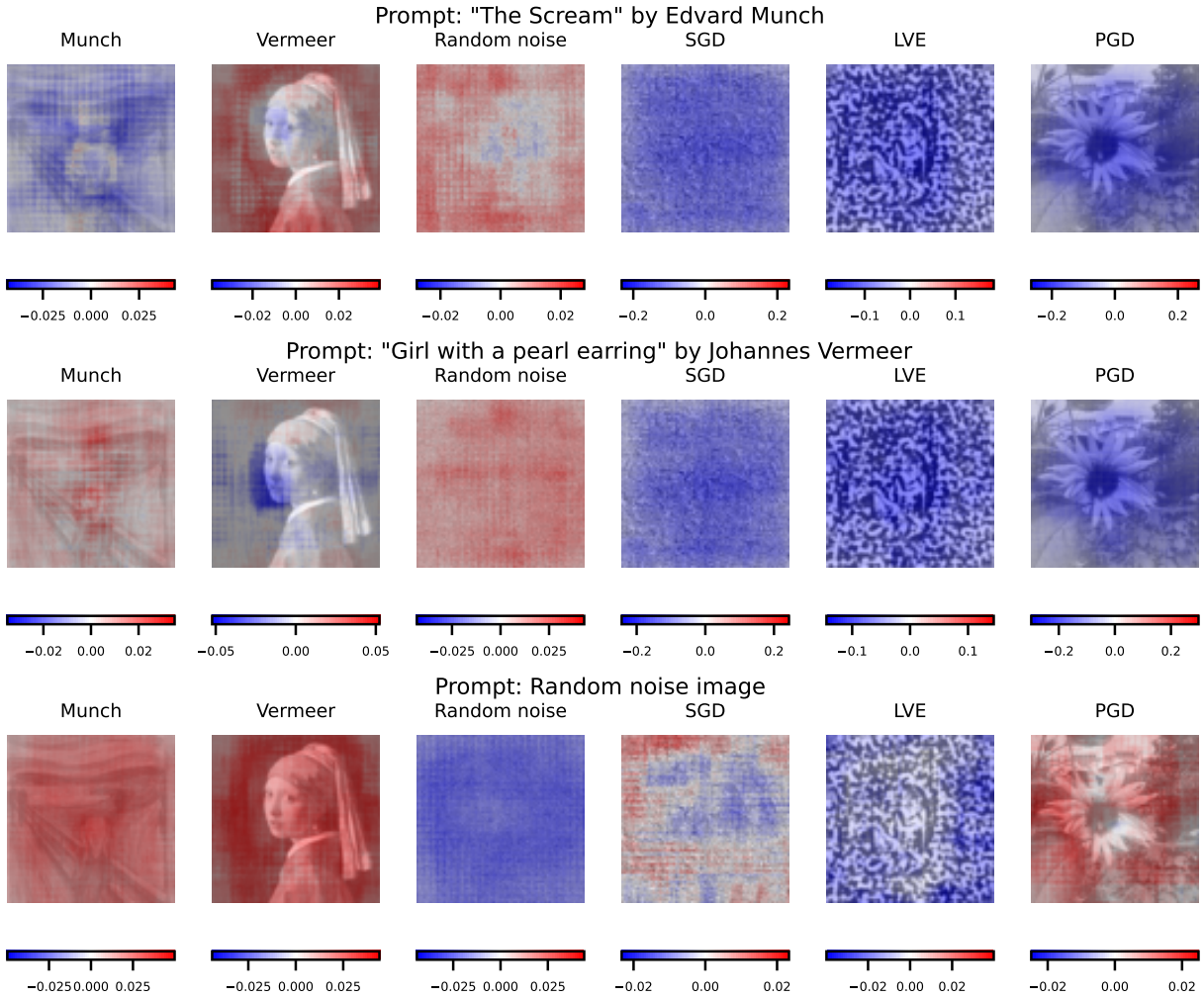

Figure 7: Occlusion maps for famous artworks, random noise baseline, and mined fooling master images for different prompts. Note that, while each row shows the same fooling master images, occlusion maps vary for different prompts. Increases in cosine similarities when blurring out a certain part of the image are denoted in red, decreases are shown in blue. Information in the fooling master images is distributed over the whole image; no individual regions in the image that can be mapped to a particular prompt.

Algorithm 1 Black-box approach to find CLIPMasterPrints

Input: initial vector $\mathbf{h}_0 \sim \mathcal{N}(0,1)$,
list of objective prompts $c_1, c_2, \ldots, c_n$,
number of to-be-run iterations i_{max}
pre-trained CLIP model $\mathcal{C}_{\theta_1}$
pre-trained image decoder $\mathcal{D}_{\theta_2}$
Initialize CMA-ES with $\mathbf{h}_0$
for i = 1 **to** $i_{\max}$ **do**
  Generate candidates $\mathbf{h}_1$,$\mathbf{h}_2$, ..., $\mathbf{h}_n$ using CMA-ES mutation
  Decode images $\mathbf{x}_1$, $\mathbf{x}_2$,...,$\mathbf{x}_n$ from $\mathbf{h}_1$, $\mathbf{h}_2$, ..., $\mathbf{h}_n$ using $\mathcal{D}_{\theta_2}$
  for all $\mathbf{x}_j$ **in** $\mathbf{x}_1$, $\mathbf{x}_2$, ..., $\mathbf{x}_n$ **do**
    Set $s_{j,\min} = \infty$
    for all c_k **in** $c_1, c_2, \ldots, c_n$ **do**
      Set $s_{j,k} = \mathcal{C}_{\theta_1}(\mathbf{x}_j, c_k)$
      if $s_{j,k} < s_{j,\min}$ **then**
        Set $s_{j,\min} = s_{j,k}$
      end if
    end for
  end for
  Update CMA-ES statistics with $s_{1,\min}$, $s_{2,\min}$, ..., $s_{n,\min}$
end for